Research Square

Preprints are preliminary reports that have not undergone peer review.
They should not be considered conclusive, used to inform clinical practice,
or referenced by the media as validated information.

Friction–wear antagonism in suspension-HVOF alumina–fluorapatite coatings on 316L stainless steel: sacrificial third-body lubrication and wear-based lifetime estimation

Halima Ghorbel
Université de Versailles Saint-Quentin-en-Yvelines
Radouane Akrache
radouane.akrache@uvsq.fr

Université de Versailles Saint-Quentin-en-Yvelines
Jinan Charafeddine
Ecole Supérieure d'Ingénieurs Léonard de Vinci
Awatef Guidara
École nationale d'Ingénieurs de Sfax

Research Article

Keywords: Fluorapatite, Alumina, Suspension HVOF, Sliding wear, Third body, Wear-based lifetime

Posted Date: November 25th, 2026

DOI: https://doi.org/10.21203/rs.3.rs-11653315/v1

License: This work is licensed under a Creative Commons Attribution 4.0 International License.
Read Full License

Additional Declarations: No competing interests reported.

Friction–wear antagonism in suspension-HVOF alumina–fluorapatite coatings on 316L stainless steel: sacrificial third-body lubrication and wear-based lifetime estimation

Halima Ghorbel[1]*, Radouane Akrache[2]*, Jinan Charafeddine[3], Awatef Guidara[4]

*[1] Laboratoire Atmosphères, Milieux, Observations Spatiales (LATMOS), UVSQ, France · [2] Laboratoire d'Ingénierie des Systèmes de Versailles (LISV), UVSQ, France · [3] De Vinci Higher Education, De Vinci Research Center, Paris, France · [4] Laboratoire des Matériaux Avancés, ENIS, Sfax, Tunisia · *Corresponding authors: halima.ghorbel-feki@uvsq.fr; radouane.akrache@uvsq.fr*

Highlights

- Adding 1 wt% fluorapatite lowers the friction of S-HVOF alumina from 0.65 to 0.55
- The same addition raises the specific wear rate by 45% and porosity by 35%
- Wear per unit of frictional energy rises by 72% and scales with inverse hardness
- Hardness drops by 43%, far more than porosity alone can explain
- At equal wear depth, the 1 wt% Fap coating lasts about 31% less sliding distance

Abstract

Alumina (Al_2O_3) and alumina–fluorapatite (Al_2O_3–Fap) coatings containing 0, 0.25, 0.5 and 1 wt% Fap were deposited on 316L stainless steel by suspension high-velocity oxy-fuel (S-HVOF) spraying and tested in dry sliding against alumina balls (5 N, 0.1 $m \cdot s^{-1}$, 400 m, three tests per composition). With increasing Fap content, the steady-state friction coefficient decreased from 0.65 to 0.55, whereas porosity increased from 4.96 to 6.71 % and the specific wear rate from 3.1×10^{-5} to 4.5×10^{-5} $mm^3 \cdot N^{-1} \cdot m^{-1}$. To separate friction from wear, an energy wear coefficient, defined as the wear volume per unit of frictional energy, was calculated. It increased by 72 % between pure alumina and the 1 wt% Fap coating, in close proportion to the decrease in Vickers hardness from 556 to 319 HV: the product of the two quantities varied by less than ±4 % across the four compositions. The lower friction thus only partly offsets the loss of hardness. This loss is much larger than the small Fap fraction or the porosity increase can account for, and is attributed to weaker cohesion between splats. The worn surfaces showed smoothed plateaus crossed by fine cracks, with fine debris and no delamination. Wear-based lifetimes were estimated from Archard's law for critical wear depths of 10 and 20 µm, with Monte Carlo propagation of the wear-rate scatter: the 1 wt% Fap coating reached a given depth after about 31 % less sliding than pure alumina. These dry-sliding data provide a reference for future tribo-corrosion tests in simulated body fluid.

Keywords: *Fluorapatite; Alumina; Suspension HVOF; Sliding wear; Third body; Wear-based lifetime*

1. Introduction

AISI 316L stainless steel remains widely used for orthopaedic and osteosynthesis devices because it combines adequate strength, formability, low cost and acceptable biocompatibility [1, 2]. Its limited resistance to wear and to wear-assisted corrosion, however, exposes 316L components to debris generation, metal-ion release and, in contacts subjected to sliding or micromotion, progressive loosening [3, 4]. Titanium and cobalt-based alloys, and increasingly ceramics, are therefore preferred for load-bearing articulating surfaces [5], and the

surface of 316L has been modified by nitriding, ion implantation, and cold-sprayed or HVAF-sprayed coatings to improve its wear behaviour [6–9].

Thermally sprayed ceramic coatings combine the toughness of the metallic substrate with a hard, chemically inert surface. Alumina is the reference wear-resistant ceramic coating, and suspension-based high-velocity flame spraying (HVSFS, or S-HVOF) produces finer and denser alumina microstructures than conventional powder spraying, with improved sliding-wear resistance [10, 11]. Calcium phosphates add bioactivity: fluorapatite ($Ca_{10}(PO_4)_6F_2$, Fap) is chemically and thermally more stable than hydroxyapatite, and alumina–Fap coatings produced by atmospheric plasma spraying have shown good adhesion and a favourable bone response in vivo [12–14]. The abrasion resistance of such composites depends on the hardness, size and distribution of the second phase relative to the contact [15].

Adding a soft or lubricious second phase to a hard sprayed coating rarely improves friction and wear at the same time. In HVOF-sprayed WC–Co–Cr coatings, for example, graphene nanoplatelet additions changed hardness, sliding wear and three-body abrasion in ways that were not uniformly beneficial [16, 17]. In such systems the secondary phase tends to lower interfacial shear, while the defects it introduces favour material removal. For S-HVOF Al_2O_3–Fap coatings, a lower friction coefficient and a higher wear rate with increasing Fap content were first reported in the doctoral thesis in which these coatings were developed [18], and the friction and wear data analysed here come from that work. The thesis did not, however, explain why the two trends coexist, nor what they imply for coating durability.

The present study addresses three points for S-HVOF Al_2O_3 and Al_2O_3–Fap coatings (0.25–1 wt% Fap) on 316L tested in dry sliding against alumina: (i) how a lower friction coefficient can coexist with a higher wear rate in the same coating; (ii) which property change controls the wear increase; and (iii) how much wear-based lifetime is lost in exchange for the lower friction. Friction and wear are separated with an energy wear coefficient [19]; the wear increase is compared with Archard [20] and lateral-fracture [21] scaling; and lifetime is estimated from Archard kinetics with an explicit critical wear depth and Monte Carlo propagation of the measured scatter. Because dry sliding does not reproduce physiological conditions, the results are intended as a reference for later tribo-corrosion work.

2. Materials and methods

2.1 Raw materials and suspension preparation

α-Alumina (α-Al_2O_3) powder (Medicoat, purity 98.9 %) was used as received. Fluorapatite was synthesised by aqueous precipitation [14] from analytical-grade $Ca(NO_3)_2{\cdot}4H_2O$, $(NH_4)_2HPO_4$ and NH_4F. The calcium nitrate solution was added dropwise to a boiling diammonium hydrogen phosphate solution under continuous stirring, the pH being kept at 9 by addition of 28 % NH_4OH. The precipitate was aged at 80 °C for 1 h, filtered, rinsed, dried at 70 °C for 12 h and calcined at 500 °C to obtain phase-pure fluorapatite [18].

Composite feedstocks containing 0.25, 0.5, and 1 wt% Fap were prepared by manually mixing α-Al_2O_3 and Fap in an agate mortar, followed by wet milling in ethanol for 10 min. The resulting slurries were dried at 80 °C for 24 h. Pure α-Al_2O_3 was processed under identical conditions and used as a reference. Suspensions for spraying were prepared by dispersing the milled powders in water at a solid loading of 10 wt%, with the addition of 0.8 wt% ammonium polymethacrylate (PMA) as a dispersant.

2.1.1 Feedstock characterisation

Particle size distributions were measured by laser diffraction (Mastersizer 3000, Malvern Panalytical). The as-received α-Al_2O_3 powder had D50 and D90 values of 34 and 52 µm (Fig. 1a). After wet milling, the composite feedstocks containing 0.25, 0.5 and 1 wt% Fap showed bimodal distributions, with a dominant fine population centred around 5 µm and a smaller coarse population extending to about 75 µm (Fig. 1b). Their D50 ranged from about 15 to 20 µm, with D10 and D90 of about 5 and 75 µm, respectively.

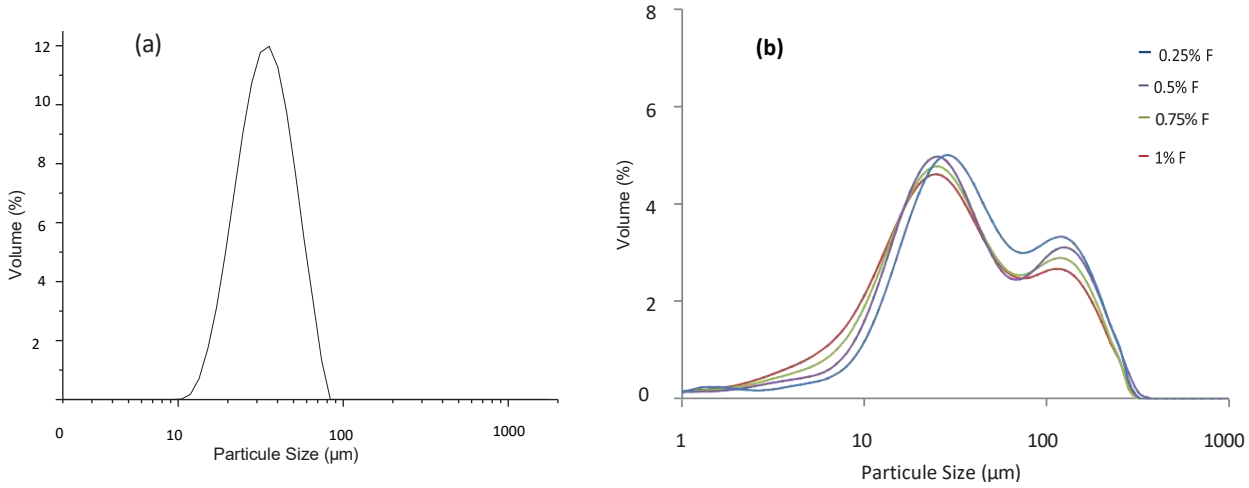


Fig. 1 Particle size distributions of (a) the as-received α-Al_2O_3 powder and (b) the milled Al_2O_3–Fap composite feedstocks.

Powder morphology was examined by SEM (JEOL JSM-5800LV, Japan) (Fig. 2). The α-Al_2O_3 particles show the angular morphology of fused-and-crushed powders, whereas the Fap particles are irregular and equiaxed, as expected from the precipitation route.

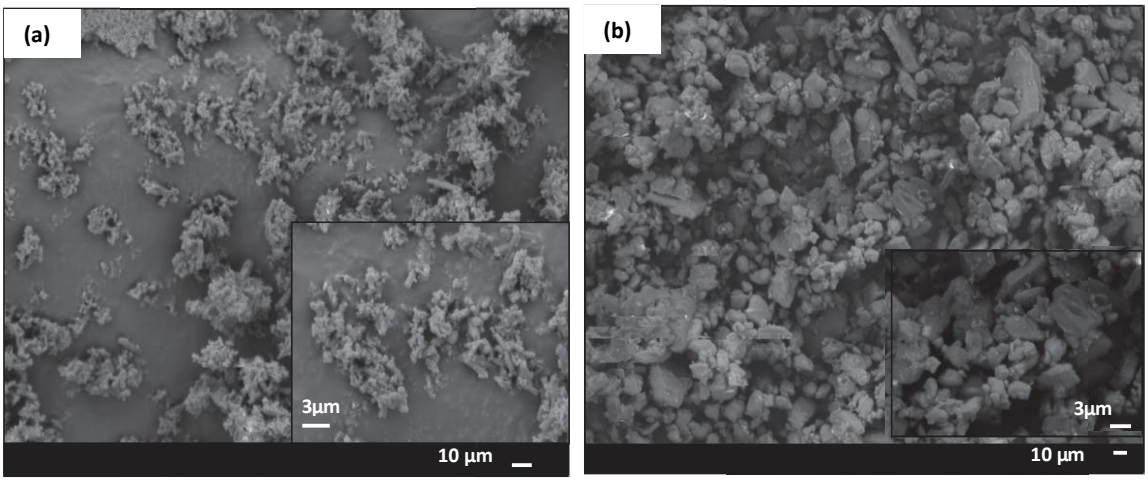


Fig. 2 SEM micrographs of the feedstock powders: (a) as-received α-Al_2O_3, showing angular fused-and-crushed morphology; (b) synthesised fluorapatite, showing irregular equiaxed particles. Main frames at ×1000 with 10 µm scale bars; insets at higher magnification with 3 µm scale bars.

2.2 Coating deposition

Coatings were deposited on 316L stainless steel substrates by suspension high-velocity oxy-fuel (S-HVOF) spraying. In this process the feedstock is dispersed in a liquid and injected as a suspension into the combustion jet, which evaporates the liquid and heats and accelerates the fine particles toward the substrate [10, 11]. The spray parameters are listed in Table 1. Before spraying, the substrates were grit-blasted at 3 bar, which raised their roughness Ra from 0.60 to 2.98 µm. The coating thickness, measured on cross-sections, was about 200 ± 15 µm for all compositions.

Table 1. Suspension HVOF (S-HVOF) spray parameters.

PARAMETER	S-HVOF
Torch manufacturer and model	Sulzer Metco CDS-8944
Spraying process	Suspension High-Velocity Oxy-Fuel (S-HVOF)
Spraying material	Al_2O_3 and Al_2O_3–Fap (0.25, 0.5, 1 wt%) suspensions
Fuel gas	CH_4
CH_4 flow rate (l min^{-1})	135
O_2 flow rate (l min^{-1})	270
Carrier gas	N_2
Carrier gas flow rate (l min^{-1})	25
Suspension feed rate (ml min^{-1})	50
Suspension solid loading (wt%)	10
Stand-off distance (mm)	165
Rotating table speed (rpm)	300
Traverse pitch (mm)	2.5
Number of passes	70
Grit-blasting pressure (bar)	3
Substrate material	316L stainless steel
Initial Substrate Roughness, Ra (µm)	0.60
Roughness After Grit Blasting, Ra (µm)	2.98

2.3 Microstructural and mechanical characterisation

Polished cross-sections were examined by optical microscopy and by SEM (JEOL JSM-5800LV). Porosity was quantified with ImageJ (NIH, USA) by grey-level thresholding of SEM micrographs taken at ×1000 (Fig. 3). About ten non-overlapping fields were analysed on each of three to five independent cross-sections per composition,

and porosity is reported as the mean ± standard deviation over all fields. Surface roughness was measured with a white-light profilometer (ALTISURF 500) and a Mitutoyo contact profilometer, and the roughness parameters were evaluated according to ISO 4287 [22].

Vickers microhardness was measured on polished cross-sections with a LEICA M09 hardness tester and a standard Vickers diamond pyramid (136°), under a load of 4.9 N (HV0.5) and a dwell time of 15 s. Five indents were made per coating. To limit the influence of porosity, indents were placed in pore-free areas, and indents whose diagonals met a pore or an inter-splat crack were discarded. The Young's modulus was determined independently using nanoindentation measurements.

2.4 Tribological testing

Dry sliding tests were carried out on a CSEM ball-on-disk tribometer (Switzerland) under the conditions listed in Table 2. Samples and balls were cleaned with ethanol before testing. Each composition was tested three times (n = 3), each time with a new ball, and results are reported as mean ± standard deviation. The steady-state friction coefficient μ_{ss} was averaged from 1000 cycles to the end of the test.

Table 2. Dry-sliding test protocol.

Parameter	**Value**
Configuration	Ball-on-disk, unidirectional rotation
Counter body	α-Al_2O_3 ball, Ø 6 mm (R = 3 mm);
Coating surface condition	As-sprayed (unpolished)
Normal load	5 N
Initial Hertzian pressure (nominal)	≈ 1.5 GPa (smooth-surface estimate, contact radius ≈ 40 µm)
Track radius	25 mm
Sliding speed	0.1 $m \cdot s^{-1}$
Sliding distance	400 m (≈ 2 550 revolutions)
Environment	Laboratory air, 20 °C, no lubricant
Wear volume measurement	3D white-light profilometry (ALTISURF 500); 5 transverse profiles per track at equally spaced angular positions
Wear rate basis	Coating (disk) volume loss; ball wear was considered negligible.
Repeats	n = 3 per composition

The specific wear rate k ($mm^3 \cdot N^{-1} \cdot m^{-1}$) was calculated as

$$k = \frac{V}{F \cdot d} \qquad (1)$$

where V is the worn volume (mm^3), F the normal load (N) and d the sliding distance (m). V was obtained from the 3D topography of each track. Five transverse profiles were extracted at equally spaced angular positions, the cross-sectional area below the mean line of the adjacent unworn surface was integrated for each profile and the mean area was multiplied by the track perimeter 2πr = 157.1 mm. The standard deviation of the five

areas was used to check that the track was uniform around the circumference. The track width w (0.24–0.27 mm) and maximum depth h (2.5–3.1 µm) were taken from the same profiles.

2.5 Friction–wear decoupling and wear-based lifetime estimation

Friction and wear were decoupled with the energy approach [19]. The frictional energy dissipated per unit sliding distance is $\mu_{ss}F$, so that the worn volume can be written $V = \alpha\mu_{ss}Fd$, where α ($mm^3 \cdot J^{-1}$) is the volume removed per unit of dissipated energy. Comparing with Eq. (1) gives

$$\alpha = \frac{k}{\mu_{ss}} \qquad (2)$$

A decrease in μ_{ss} lowers the energy supplied to the contact, whereas an increase in α indicates a lower resistance of the coating to removal by that energy.

Wear-based lifetime was estimated from Archard kinetics [20]. At constant specific wear rate, the worn volume after N revolutions is

$$V(N) = k \cdot F \cdot 2\pi r \cdot N \qquad (3)$$

End of life is defined as the moment when the maximum wear depth reaches a critical value h_{crit}. The corresponding critical volume is obtained by assuming that the track cross-section follows the profile of the unworn ball, i.e. a circular segment of radius R = 3 mm:

$$V_{\mathrm{crit}} = 2\pi r \left[R^2 \arccos\left(\frac{R - h_{\mathrm{crit}}}{R}\right) - (R - h_{\mathrm{crit}})\sqrt{2Rh_{\mathrm{crit}} - h_{\mathrm{crit}}^2} \right] \qquad (4)$$

Ball wear or flattening widens the track and reduces the depth reached for a given volume. Equation (4) therefore gives the smallest volume, and hence the shortest lifetime, compatible with a given h_{crit}, i.e. a conservative estimate; this assumption is checked against the measured track profiles in Section 3.3. Two functional criteria were used: h_{crit} = 10 µm and 20 µm, i.e. 5 % and 10 % of the nominal coating thickness. Wear through the full 200 µm thickness was not considered, because it would require extrapolating the 400 m tests by more than two orders of magnitude. Combining Eqs. (3) and (4), the sliding distance and number of revolutions to end of life are

$$d_{\mathrm{crit}} = \frac{V_{\mathrm{crit}}}{k \cdot F}, \quad N_{\mathrm{crit}} = \frac{d_{\mathrm{crit}}}{2\pi r} \qquad (5)$$

The scatter in k was propagated by Monte Carlo sampling (2×10^5 draws per composition) from a log-normal distribution with the measured mean and a coefficient of variation of 12 %, the largest value observed among the compositions. The median and the 2.5–97.5 percentile interval of d_{crit} are reported; they describe the test-to-test scatter expected for an individual coating. The estimates assume that the steady-state wear rate measured over 400 m remains constant up to d_{crit}, an extrapolation by a factor of about 6 to 24, and are valid only for the conditions of Table 2.

3. Results

3.1 Porosity

Porosity increased progressively with Fap content, from 4.96 ± 0.30 % for Al_2O_3 to 6.71 ± 0.30 % for Al_2O_3–1 wt% Fap (Table 3; procedure in Fig. 3). This increase cannot be explained by the melting behaviour of bulk fluorapatite alone (≈ 1650 °C [23]). In the S-HVOF jet, the minor Fap phase more likely modifies the melting, flattening and solidification of composite particles locally, and weakens splat-to-splat contact, so that even small additions affect inter-splat bonding [13]. The rounded pores in Fig. 3 are consistent with localised liquid formation followed by rapid solidification.

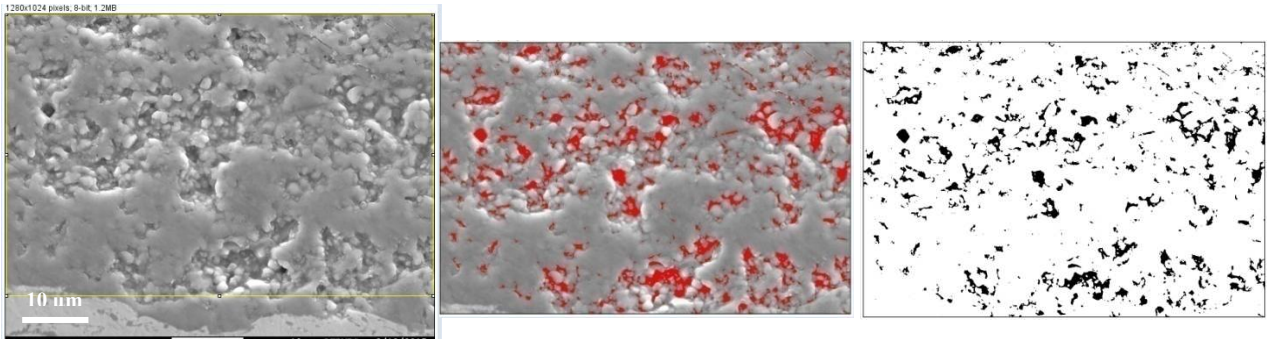


Fig. 3 Image-processing procedure used for porosity quantification, illustrated on a polished cross-section of an Al_2O_3–Fap coating: (left) SEM micrograph at ×1000; (centre) segmented porosity overlaid in red; (right) binary mask used for area-fraction measurement.

3.2 Friction

Fig. 4 shows the friction coefficient against the alumina ball as a function of sliding cycles. All coatings start at about 0.2–0.3 and reach a steady state after a running-in period. μ_{ss} decreases monotonically with Fap content, from 0.64 ± 0.05 for Al_2O_3 to 0.58 ± 0.03, 0.56 ± 0.04 and 0.54 ± 0.03 for 0.25, 0.5 and 1 wt% Fap (Table 3), a reduction of about 15 %. The coefficient of variation of μ_{ss} remained below 8 % for all compositions. The curves in Fig. 4 show one representative test per composition, so their plateaus differ slightly from the means over three tests given in Table 3. The initial rise of friction during running-in is commonly associated with the removal of surface contaminants and the fracture of asperities, which establishes a debris-laden contact.

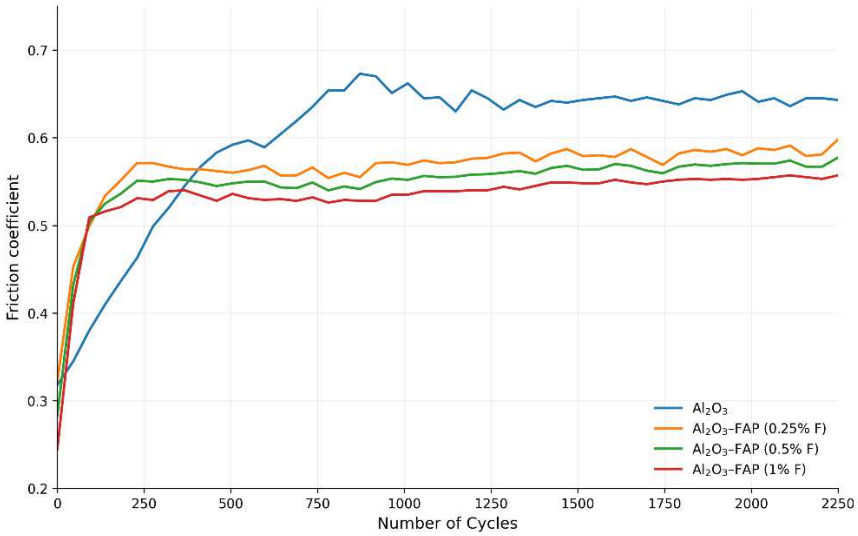


Fig. 4 Friction coefficient against an alumina ball as a function of sliding cycles for Al_2O_3 and Al_2O_3–Fap coatings on 316L stainless steel (5 N, 0.1 $m \cdot s^{-1}$).

3.3 Wear rate and wear-track geometry

Specific wear rates after 400 m are given in Fig. 5 and Table 3. k increases monotonically with Fap content, from 3.1×10^{-5} $mm^3 \cdot N^{-1} \cdot m^{-1}$ for Al_2O_3 to 3.6, 4.0 and 4.5×10^{-5} $mm^3 \cdot N^{-1} \cdot m^{-1}$ for 0.25, 0.5 and 1 wt% Fap (+45 %). The coefficient of variation remained below 12 % for all compositions, and the mean worn volumes range from 0.062 to 0.090 mm^3.

The mean track width w and maximum depth h measured on the transverse profiles are reported in Table 3. Track width ranged from [w] µm for Al_2O_3 to [w] µm for Al_2O_3–1 wt% Fap, and maximum depth from [h] to [h] µm. If the worn cross-section followed the profile of the unworn ball (R = 3 mm), as assumed in Eq. (4), the measured volumes would correspond to widths of 0.24–0.27 mm and depths of 2.4–3.1 µm. The measured tracks are wider and shallower than this ideal profile, which indicates flattening of the ball tip and lateral spreading of the contact by debris. For a given worn volume, the ideal profile therefore overestimates the depth, so the lifetimes derived from Eq. (4) in Section 3.5 are conservative. The depths reached after 400 m are of the same order as the roughness of the as-sprayed surface (Ra ≈ 3.4–3.7 µm, Table 3), so they carry a large relative uncertainty. The worn volume, which integrates the whole cross-section, is the more robust quantity and was used for all subsequent calculations.

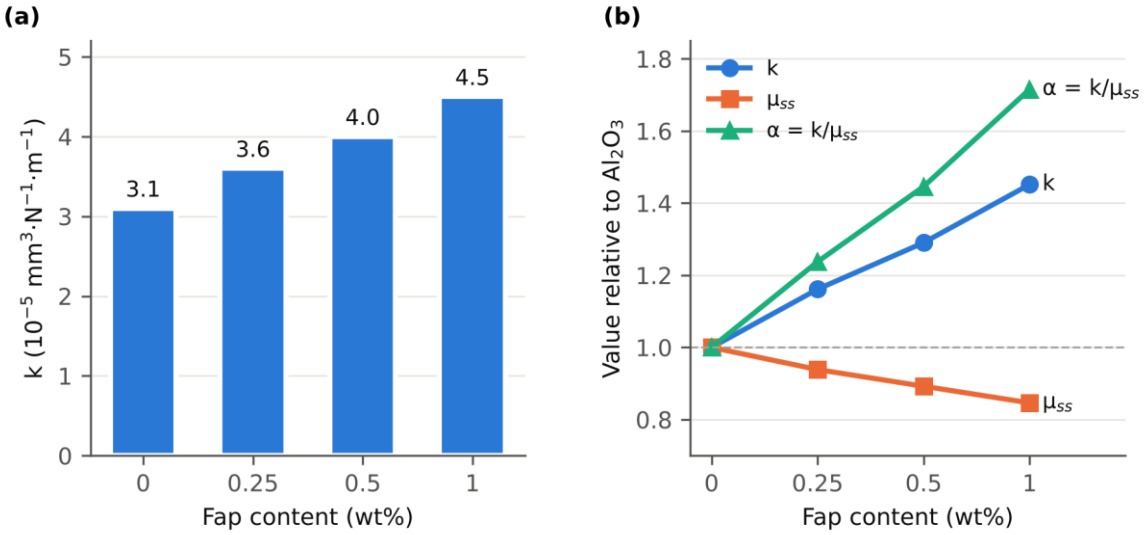


Fig. 5 (a) Specific wear rate k of Al_2O_3 and Al_2O_3–Fap coatings on 316L stainless steel after 400 m of dry sliding at 5 N (means of n = 3 tests). (b) Steady-state friction coefficient μ_{ss}, specific wear rate k and energy wear coefficient $\alpha = k/\mu_{ss}$, relative to Al_2O_3.

Table 3. Microstructural, mechanical and tribological properties of the coatings. $\alpha = k/\mu_{ss}$ is the energy wear coefficient (Eq. 2). w and h are the mean track width and maximum depth after 400 m, measured on the transverse profiles (Section 2.4).

Coating	Porosity (%)	Ra (µm)	HV	E (GPa)	μ_{ss}	k (10^{-5} mm³·N⁻¹·m⁻¹)	α (10^{-5} mm³·J⁻¹)
Al_2O_3	4.96 ± 0.30	3.42 ± 0.15	556 ± 39	59.7	0.64 ± 0.05	3.1	4.8
Al_2O_3–0.25 wt% Fap	5.28 ± 0.40	3.51 ± 0.18	447 ± 42	62.9	0.58 ± 0.03	3.6	5.9
Al_2O_3–0.5 wt% Fap	5.94 ± 0.40	3.57 ± 0.20	361 ± 42	82.6	0.56 ± 0.04	4.0	6.9
Al_2O_3–1 wt% Fap	6.71 ± 0.30	3.66 ± 0.22	319 ± 44	98.3	0.54 ± 0.03	4.5	8.2

3.4 Worn surfaces

SEM views of the wear tracks are shown in Fig. 6. At low magnification all tracks are continuous and relatively smooth, without large-scale spallation or lamellar delamination of splats. At higher magnification, the worn surfaces consist of smoothed plateaus separated by a network of fine cracks, most visible on the Al_2O_3–0.25 wt% Fap track (Fig. 6b, right) with fine particulate debris along the cracks and dispersed on the plateaus. Fine debris appears more abundant on the 1 wt% Fap track (Fig. 6d, right). In Fig. 6c, the boundary between a worn plateau and an unworn, rougher area shows that wear proceeds by progressive smoothing and fragmentation of asperities. From SEM observation alone, the fine debris cannot be attributed unambiguously to the Fap phase; its likely origin is discussed in Section 4.3.

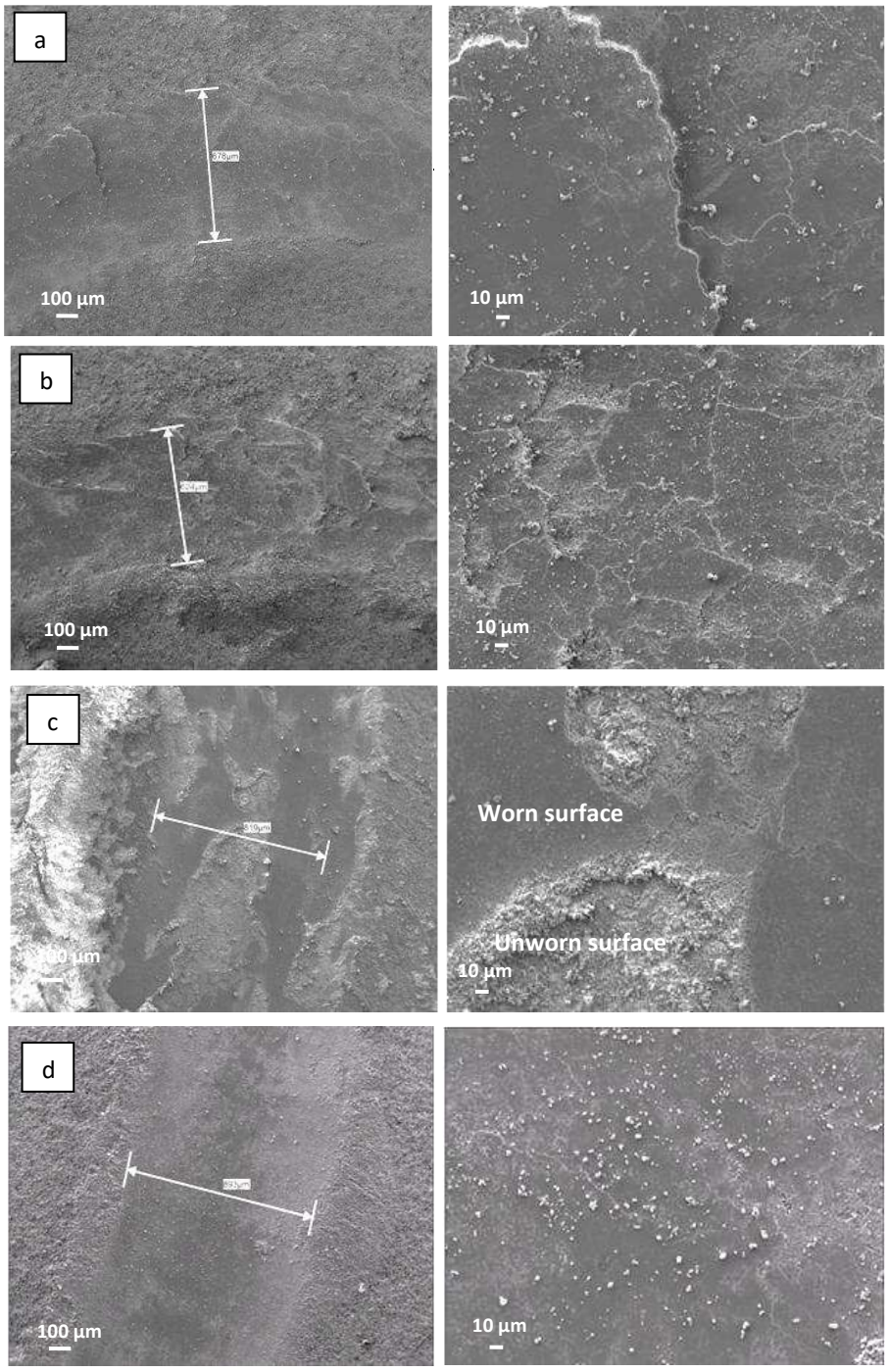


Fig. 6 SEM views of the wear tracks: (a) Al_2O_3, (b) Al_2O_3–0.25 wt% Fap, (c) Al_2O_3–0.5 wt% Fap, (d) Al_2O_3–1 wt% Fap. Left: track overview with width indicated (100 µm scale bars). Right: detail of the worn surface (10 µm scale bars). In (c), the boundary between worn and unworn regions is indicated.

3.5 Wear-based lifetime estimates

Eq. (4) gives critical volumes of 0.51 mm³ for h_{crit} = 10 µm (track width 0.49 mm) and 1.45 mm³ for h_{crit} = 20 µm (track width 0.69 mm). The resulting lifetimes are listed in Table 4. For h_{crit} = 20 µm, the Al_2O_3 coating reaches end of life after about 9.4 km of sliding (≈ 60 × 10³ revolutions), and the Al_2O_3–1 wt% Fap coating after about 6.5 km (≈ 41 × 10³ revolutions). Because d_{crit} is proportional to 1/k at fixed V_{crit}, the lifetime relative to alumina does not depend on the criterion: it falls to 0.86, 0.78 and 0.69 for 0.25, 0.5 and 1 wt% Fap. With the

conservative 12 % scatter assumed for k, the 95 % intervals of adjacent compositions overlap widely, and even those of Al_2O_3 and Al_2O_3–1 wt% Fap overlap slightly.

Table 4. Estimated sliding distance d_{crit} (km; median [95 % interval]) and number of revolutions N_{crit} (10^3; median) to reach the critical wear depth, from Eqs. (4)–(5) with Monte Carlo propagation of the scatter in k (CV = 12 %).

Coating	k (10^{-5} $mm^3 \cdot N^{-1} \cdot m^{-1}$)	h_{crit} = 10 µm: d_{crit} / N_{crit}	h_{crit} = 20 µm: d_{crit} / N_{crit}	Relative lifetime
Al_2O_3	3.1	3.33 [2.63–4.21] / 21.2	9.42 [7.45–11.91] / 60.0	1.00
Al_2O_3–0.25 wt% Fap	3.6	2.87 [2.27–3.63] / 18.3	8.11 [6.41–10.24] / 51.6	0.86
Al_2O_3–0.5 wt% Fap	4.0	2.58 [2.04–3.26] / 16.4	7.30 [5.78–9.22] / 46.4	0.78
Al_2O_3–1 wt% Fap	4.5	2.29 [1.81–2.90] / 14.6	6.49 [5.13–8.21] / 41.3	0.69

4. Discussion

Adding Fap thus produces two opposing trends, a 15 % reduction in friction and a 45 % increase in wear rate, together with a 35 % increase in porosity and a 43 % decrease in hardness. Section 4.1 separates friction from wear, Section 4.2 relates the wear increase to the loss of hardness and discusses the origin of that loss, Section 4.3 deals with the role of the debris and Section 4.4 with coating durability.

4.1 Decoupling friction from wear

The friction coefficient reflects the shear resistance of the interface, whereas the specific wear rate reflects how much material leaves the coating per unit load and distance. A third body can lower the former while raising the latter. The energy wear coefficient $\alpha = k/\mu_{ss}$ (Eq. 2) separates the two contributions. The frictional energy dissipated per unit sliding distance decreases with Fap content in proportion to μ_{ss} (−15 % at 1 wt%), while the volume removed per joule increases from 4.8×10^{-5} to 8.2×10^{-5} $mm^3 \cdot J^{-1}$ (+72 %, Table 3). The 45 % increase in k is the product of these two factors ($0.85 \times 1.72 \approx 1.45$). Fap-containing coatings therefore receive less frictional energy but are much less resistant to removal by that energy.

Such behaviour is expected when the lubricating debris is produced by the coating itself. In the third-body description of dry contacts, debris that is continuously generated and partly ejected from the contact both carries load and constitutes wear [24, 25]. Lower friction and faster wear can then result from the same process, the fracture-driven release of fine particles. α combines the cumulative wear rate over 400 m with the steady-state friction coefficient. Running-in lasts longer for Al_2O_3 than for the Fap-containing coatings (Fig. 4); since running-in wear is usually higher than steady-state wear, the measured k of pure alumina is, if anything, overestimated, and the increase with Fap content underestimated.

4.2 Origin of the wear increase

Between Al_2O_3 and Al_2O_3–1 wt% Fap, the Vickers hardness falls from 556 to 319 HV (5.45 to 3.13 GPa), i.e. by 43 %. Under Archard's law ($k \propto 1/H$), this alone would raise the wear rate by 74 %, more than the 45 % measured. The energy wear coefficient, on the other hand, follows the hardness closely. For 0.25, 0.5 and 1

wt% Fap, α increases by 24, 45 and 72 %, while 1/H increases by 24, 54 and 74 %, and the dimensionless product αH remains between 2.44×10^{-4} and 2.60×10^{-4} for the four coatings (within ±4 % of its mean). The volume removed per joule of frictional energy is therefore governed by hardness, and the lower friction of the Fap-containing coatings recovers part of what the hardness loss costs: $1.74 \times 0.85 \approx 1.48$, close to the measured ratio of 1.45.

Lateral-fracture models, in which the wear volume also depends on E/H and on fracture toughness [21], do not improve this description: with the indentation moduli of Table 3, which increase with Fap content, they would predict a much larger wear increase than observed. Together with the absence of spallation on the worn tracks (Fig. 6), this suggests that material is removed mainly by fine-scale abrasion and fragmentation rather than by lateral cracking.

The loss of hardness itself needs an explanation. A Fap content of 1 wt% corresponds to about 1.2 vol%, far too little to lower the hardness through a rule-of-mixtures effect. Porosity contributes, but only in part: with the exponential dependence of hardness on porosity usually reported for ceramics, $H \propto \exp(-bP)$ with b = 4–9 [26], the porosity increase of 1.75 percentage points would lower the hardness by 7–15 %, whereas a 43 % decrease would require $b \approx 32$. Across the four compositions, k correlates linearly with porosity ($k = 0.75P - 0.51$, with k in 10^{-5} $mm^3 \cdot N^{-1} \cdot m^{-1}$ and P in %; $r = 0.98$, $n = 4$), but porosity is almost collinear with Fap content ($r = 0.99$), so this correlation cannot separate the effect of the pores from that of the phase that creates them.

The most likely cause is weaker cohesion between splats. As discussed in Section 3.1, the minor Fap phase probably alters the melting and flattening of the composite particles and degrades inter-splat bonding. Poorly bonded splat boundaries lower the resistance to indentation, and they are also the paths followed by the fine crack network seen on the worn surfaces (Fig. 6), whose fracture releases fine debris. If this interpretation is correct, the indentation fracture toughness of the coatings [27] should also decrease with Fap content, and measuring it would provide a direct test.

4.3 Third-body debris and the role of Fap

The friction reduction is attributed to a layer of fine debris that accommodates the velocity difference between ball and coating and lowers the effective interfacial shear stress [24, 25]. Three observations point to a contribution of Fap to this layer: friction decreases steadily with Fap content, fine debris is more abundant on Fap-rich tracks (Fig. 6), and fluorapatite is much softer and more easily comminuted than dense alumina [28]. Without compositional mapping of the tracks, however, the Fap origin of the debris and the coverage of the third-body layer remain inferences, and the debris is most likely a mixture of alumina and Fap fragments.

The conclusion of Section 4.1 does not depend on this attribution. Whatever its composition, the debris that lowers friction is produced by fracture of the coating, so its lubricating action cannot be separated from the wear increase. Comparable antagonistic effects of a soft or lubricious secondary phase have been reported for HVOF-sprayed carbide coatings containing graphene [16, 17].

4.4 Implications for coating durability

In terms of lifetime (Table 4), lowering μ_{ss} by 15 % with 1 wt% Fap shortens the estimated wear-based lifetime by about 31 % for a given critical depth. Intermediate contents follow the same pattern, with lifetime reductions of 14 % and 22 % for friction reductions of 6 % and 11 %. Within the range studied, no composition improves friction without a more than proportional loss of wear life. Whether this is acceptable depends on the function of the surface. Where Fap is added mainly for bioactivity and bone bonding [14], the lowest Fap content that meets the biological requirement should be preferred from a wear standpoint, whereas a friction-limited application might accept a shorter life.

The lifetime estimates rely on a steady-state wear rate extrapolated by a factor of about 6–24 beyond the tested distance and on a conservative track geometry. They rank the compositions reliably, since this ranking depends only on k, but their absolute values should be confirmed by longer tests with intermediate volume measurements.

4.5 Limitations and relevance to biomedical use

Dry sliding in air at room temperature is a fundamental characterisation step and does not reproduce the conditions of articulating implant surfaces, which involve lubrication by synovial fluid, cyclic loading, pH and ionic-strength effects and protein adsorption. In addition, all compositions were sprayed with a single parameter set and tested at one load and speed, and only four compositions were studied. The correlations reported above are therefore descriptive, and the mechanistic interpretation rests on scaling arguments that should be confirmed by fracture toughness measurements and compositional analysis of the tracks. A data-driven description of wear across compositions, loads and spray conditions, as recently attempted for other thermally sprayed systems [29, 30], would require a much larger experimental matrix than the present one.

5. Conclusions

The dry-sliding behaviour of S-HVOF Al_2O_3 and Al_2O_3–Fap coatings on 316L stainless steel was characterised and analysed. The main conclusions are as follows.

- Adding 0.25–1 wt% Fap lowers the steady-state friction coefficient against alumina from 0.65 to 0.55 (−15 %) but increases the porosity from 4.96 to 6.71 % and the specific wear rate from 3.1×10^{-5} to 4.5×10^{-5} $mm^3 \cdot N^{-1} \cdot m^{-1}$ (+45 %).
- The energy wear coefficient increases by 72 %: the Fap-containing coatings dissipate less frictional energy but lose more material per joule. Lower friction and faster wear both result from the fracture-driven generation of fine debris, so that Fap acts as a sacrificial third-body lubricant.
- The Vickers hardness decreases by 43 % (556 to 319 HV), and the energy wear coefficient scales almost exactly with inverse hardness (αH constant within ±4 %). This hardness loss is too large to result from the small Fap fraction or from porosity alone and is attributed to weaker inter-splat cohesion, which remains to be confirmed by fracture toughness measurements.

- With an explicit critical-depth criterion, Archard kinetics and Monte Carlo propagation of the wear-rate scatter, the wear-based lifetime of the 1 wt% Fap coating is about 31 % shorter than that of pure alumina, independently of the chosen criterion.

Future work will (i) measure the indentation fracture toughness of the coatings and map the composition of tracks and debris to test the proposed mechanism, (ii) extend the tests to longer distances with intermediate volume measurements to validate the lifetime extrapolation, and (iii) evaluate the coatings under tribo-corrosion in simulated physiological fluids.

Declaration of competing interest

The authors declare that they have no known competing financial interests or personal relationships that could have appeared to influence the work reported in this paper.

Data availability

Data will be made available on request.

References

[1] Luo J, et al. 316L stainless steel manufactured by selective laser melting and its biocompatibility. Metals. 2018;8:548.

[2] Wang Z, et al. Decline in pitting corrosion resistance of 316L stainless steel during tribocorrosion. npj Materials Degradation. 2025;9:1–10.

[3] Fellah M, et al. Comportement à l'usure et au frottement de l'acier inoxydable AISI 316L pour applications biomédicales. Matériaux & Techniques. 2018;106:402.

[4] Yousif MAS, et al. Mechanical, tribological and corrosion behavior of L-PBF 316L stainless steel. Journal of Materials Research and Technology. 2024;33:1220–1233.

[5] Merola M, Affatato S. Materials for hip prostheses: a review of wear and loading considerations. Materials. 2019;12:495.

[6] Kao WH, Su YL. Tribological properties of biomedical 316L stainless steel after plasma nitriding and TiC:H coating. Industrial Lubrication and Tribology. 2018;70:1516–1526.

[7] Piotrowska K, et al. Functional properties of 316L steel subjected to ion implantation. Materials. 2021;14:5525.

[8] Adachi S, Ueda N. Wear and corrosion of cold-sprayed AISI 316L coatings treated by plasma carburizing and nitriding. Coatings. 2018;8:456.

[9] Wang Z, et al. Improving wear and corrosion resistance of HVAF-sprayed 316L by adding TiB_2 and CeO_2. Journal of Materials Research and Technology. 2024;31:1313–1325.

[10] Bolelli G, Rauch J, Cannillo V, Killinger A, Lusvarghi L, Gadow R. Microstructural and tribological investigation of high-velocity suspension flame sprayed (HVSFS) Al_2O_3 coatings. Journal of Thermal Spray Technology. 2009;18:35–49. doi:10.1007/s11666-008-9279-9

[11] Junge P, Heppke EM, Kleba-Ehrhardt R, Karl D, Cios G, Rupprecht C. Phase evolution and microstructure of suspension HVOF-sprayed alumina coatings. Surface and Coatings Technology. 2025;499:131885. doi:10.1016/j.surfcoat.2025.131885

[12] Ghorbel-Feki H, Guidara A, Danlos Y, Bouaziz J, Coddet C. Synthesis and characterization of alumina–fluorapatite coatings deposited by atmospheric plasma spraying. Materials Letters. 2016;185:268–271. doi:10.1016/j.matlet.2016.08.034

[13] Ghorbel-Feki H, et al. Alumina–fluorapatite composite coating deposited by atmospheric plasma spraying: an agent of cohesion between bone and prostheses. Materials Science and Engineering C. 2017;71:1090–1098.

[14] Ghorbel H, et al. Assessment of fluorapatite–alumina coating for durable adhesion of the interface prosthesis/bone cells: implementation in vivo. Journal of Medical and Biological Engineering. 2020;40:158–168.

[15] Zum Gahr KH. Wear by hard particles. Tribology International. 1998;31:587–596.

[16] Kumar V, Verma R, Shrivastava S. Microhardness and dry sliding wear behaviour of HVOF sprayed WC-Co-Cr + graphene nanoplatelets coating. Materials Today: Proceedings. 2023. doi:10.1016/j.matpr.2023.08.044

[17] Kumar V, Singh V, Bansal A, Verma R. Three-body abrasion test of HVOF sprayed WC-10Co-4Cr and WC-10Co-4Cr + 2 % graphene coating on IS-2062 steel. Diamond and Related Materials. 2024;147:111329. doi:10.1016/j.diamond.2024.111329

[18] Ghorbel-Feki H. Élaboration et caractérisation de revêtements composites (apatite–alumine) sur métal par projection thermique [PhD thesis]. Université Bourgogne Franche-Comté (UTBM), Belfort; 2016. theses.fr: 2016BELF0304; HAL: tel-01878680.

[19] Fouvry S, Liskiewicz T, Kapsa Ph, Hannel S, Sauger E. An energy description of wear mechanisms and its applications to oscillating sliding contacts. Wear. 2003;255:287–298.

[20] Archard JF. Contact and rubbing of flat surfaces. Journal of Applied Physics. 1953;24:981–988.

[21] Evans AG, Marshall DB. Wear mechanisms in ceramics. In: Rigney DA, editor. Fundamentals of Friction and Wear of Materials. Metals Park (OH): American Society for Metals; 1981. p. 439–452.

[22] ISO 4287:1997. Geometrical Product Specifications (GPS) — Surface texture: Profile method — Terms, definitions and surface texture parameters. Geneva: International Organization for Standardization; 1997.

[23] Berak J, Tomczak-Hudyma I. Phase equilibrium in the system of tricalcium phosphate–calcium fluoride. Roczniki Chemii. 1972;46:2157–2164.

[24] Godet M. The third-body approach: a mechanical view of wear. Wear. 1984;100:437–452.

[25] Berthier Y. Experimental evidence for friction and wear modelling. Wear. 1990;139:77–92.

[26] Rice RW. Porosity of Ceramics. New York: Marcel Dekker; 1998.

[27] Anstis GR, Chantikul P, Lawn BR, Marshall DB. A critical evaluation of indentation techniques for measuring fracture toughness: I, direct crack measurements. Journal of the American Ceramic Society. 1981;64:533–538.

[28] Broz ME, Cook RF, Whitney DL. Microhardness, toughness, and modulus of Mohs scale minerals. American Mineralogist. 2006;91:135–142. doi:10.2138/am.2006.1844

[29] Shabana S, et al. Towards intelligent tribology: predicting wear in WC–Co coatings with machine learning. Journal of Bio- and Tribo-Corrosion. 2025;11:88.

[30] Jagadeeshanayaka N, Negi MS, Jambagi SC. Tribological and microstructural evaluation of HVOF-sprayed hydroxyapatite coatings with machine learning-based wear rate prediction. Tribology International. 2026;213:111038.